Catalysis Surveys from Asia
https://doi.org/10.1007/s10563-021-09330-y

ORIGINAL ARTICLE

The Effects of Surface Modification of ATP on the Performance of CeO_2–WO_3/TiO_2 Catalyst for the Selective Catalytic Reduction of NO_x with NH_3

Wangwang Xie[1,2] · Guodong Zhang[1] · Bin Mu[1] · Zhicheng Tang[1,3] · Jiyi Zhang[2]

Received: 18 January 2021 / Accepted: 21 March 2021

Abstract
A series of CeO_2–WO_3/20%ATP-TiO_2 catalysts were synthesized, of which attapulgite (ATP) was modified by different methods. Notably, after ATP was dissociated and acidified, the catalyst synthesized by the impregnation method exhibited satisfactory performance for selective catalytic reduction (SCR) NO_x with NH_3. In more detail, the NO conversion could reach to 88% at 240 °C and maintain above 93% in the temperature range of 280–400 °C. Subsequently, the NO conversion of the best catalyst could keep above 80% after introducing H_2O and SO_2, so this catalyst also had strong tolerance to H_2O and SO_2 performance. Besides, the results of XRD, XPS, TEM characterizations suggested that the high dispersion of active species cerium and tungsten on the surface of ATP, which played an important role in improving the SCR performance of the catalyst. In short, the surface dissociation and surface acidification of a small amount of ATP carrier can improve the catalyst catalytic performance, so it will have a broad application prospect in SCR reaction.

Keywords CeO_2–WO_3/20%ATP-TiO_2 · Dissociation of attapulgite · Surface acidification · Strong interaction · SCR performance

1 Introduction

NO_x has been recognized as a major pollutant in the atmosphere. NO_x emission mainly originates from automobile exhaust and industrial combustion of fossil fuels. Moreover, NO_x can cause a series of environmental problems such as acid rain, ozone hole, photochemical smog, and what is more serious is causing global warming [1–4]. To remove NO_x, selective catalytic reduction of NO_x with ammonia gas (NH_3-SCR) has been widely applied [5–8]. At present, the V_2O_5–WO_3(MoO_3)–TiO_2 catalyst is widely used commercially. However, the kind of catalyst has many disadvantages, such as toxicity of vanadium species, narrow temperature window, and poor thermal stability [9], these shortcomings limit its wide application in industry. Therefore, no vanadium and with a wide temperature window catalyst has attracted great attention [10–12].

To replace vanadium, Ceria (CeO_2) is considered to be an important additive and storage of oxygen material. Meanwhile, cerium-based catalysts have many advantages such as non-toxic, superior oxygen storage capacity, and admirable redox performance, these advantages can significantly improved the catalytic performance of the catalysts [13–15]. Generally, ceria can store and release oxygen in SCR reaction, and the cerium-based catalysts exist the mutual transfer of between Ce^{3+} and Ce^{4+}. Therefore, the production of oxygen vacancies is promoted [16, 17]. Especially, by introducing ceria, the oxidation capacity from NO to NO_2 was improved, so the catalytic performance was enhanced. Li et al. [6] synthesized the CeO_2/TiO_2 catalyst by the

✉ Zhicheng Tang
tangzhicheng@licp.cas.cn

✉ Jiyi Zhang
Zhangjiyi@lut.cn

1 State Key Laboratory for Oxo Synthesis and Selective Oxidation, and National Engineering Research Center for Fine Petrochemical Intermediates, Key Laboratory of Clay Mineral Applied Research of Gansu Province, Lanzhou Institute of Chemical Physics, Chinese Academy of Sciences, Lanzhou 730000, China

2 School of Petroleum and Chemical, Lanzhou University of Technology, Lanzhou 730050, China

3 Dalian National Laboratory for Clean Energy, Dalian Institute of Chemical Physics, Chinese Academy of Sciences, Dalian 116023, China

Published online: 02 April 2021

impregnation method, and the catalyst exhibited a better catalytic activity at 280–400 °C. However, the resistance to SO_2 performance of the catalyst was not ideal. tungsten (WO_3) has been widely used in traditional vanadium-based catalysts as a promoter or stabilizers. Shan et al. [18] also synthesized the CeO_2–WO_3–TiO_2 catalyst by introducing WO_3, and it showed excellent SCR performance and strong resistance to H_2O and SO_2. Besides, the synergistic effects of CeO_2 and WO_3 can increase the acid sites and active oxygen species of catalysts, so the SCR performance was enhanced by the catalysts. Jiang et al. [19] also prepared a CeO_2–WO_3–TiO_2 catalyst, and it had superior catalytic activity and strong tolerance to H_2O and SO_2. Gao et al. [20] compared the catalytic performance of CeO_2/TiO_2 catalyst synthesized by different methods, and the experiment results exhibited that the catalyst synthesized by one-step sol–gel method had higher catalytic activity. Even so, some disadvantages existed in cerium-based catalysts. For example, the carrier is not suitable, thermal stability is poor and the specific surface area is small [21, 22]. Besides, such catalysts are easily sintered at high temperature [23]. These shortcomings limit the wide application of this kind of catalyst. Therefore, it is particularly important to find a suitable carrier for the NH_3-SCR reaction.

In recent years, the use of attapulgite (ATP) as a carrier has aroused people's great attention [24–26]. The ATP surface can form a double electron layer structure or abundant surface functional group because of the difference in pH. Furthermore, ATP as the carrier of the catalyst is more conducive to a load of rare earth active components [27–29]. Such Ce^{3+} and W(VI), which can be adsorbed on the ATP surface, and the active species are highly dispersed on the ATP surface. However, the ATP has a weak adsorption capacity to reactants (NH_3). Therefore, adding TiO_2 around the catalyst, which increases the adsorption on the reactants, and active species are exchanged or transferred within the catalyst. In our previous study, we found that only doping content 20 wt% ATP of the CeO_2–WO_3/TiO_2 catalyst can greatly improve the dispersion performance of active species, moreover, the SCR activity of the catalyst has been promoted [30]. While, the H_2O and SO_2 resistance of catalysts need to be improved. Xie et al. [31] synthesized the γ-Fe_2O_3 modified MnO_2/ATP catalyst. The NH_3-TPD and XPS results showed that the amounts of the acidic sites and surface chemisorbed oxygen were significantly enhanced after surface modification with γ-Fe_2O_3. And the interaction between metals was enhanced by using γ-Fe_2O_3 modification. All these were beneficial to improve the SCR and resistance to H_2O and SO_2 performance of the γ-Fe_2O_3/MnO_2-ATP catalyst. Chen et al. [32] prepared Cu modified attapulgite catalyst. The results suggested that 1%Cu-ATP catalyst showed good SCR performance and good H_2O and SO_2 tolerance properties. And the characterization results exhibited that Cu^{2+} increased the strong acid sites and CuO enhanced more moderate acid sites of the catalyst. Therefore, the catalytic activity of the catalyst was significantly improved. Huang et al. [29] synthesized Ce modified $MnTiO_x$/ATP catalyst by co-precipitation methods. A series of characterizations proved that the surface area, oxygen vacancy, redox ability, and acid sites of the Ce-$MnTiO_x$/ATP catalyst were significantly improved by using cerium modification. So the Ce-$MnTiO_x$/ATP catalyst exhibited excellent SCR performance and better tolerance H_2O and SO_2 properties. Therefore, through the above work, it was proposed that doping a small amount of surface-modified attapulgite was more beneficial to the SCR reaction, and could strengthen the interaction between active species.

In this work, a series of CeO_2–WO_3/20%ATP-TiO_2 catalysts were synthesized by the impregnation method, of which ATP was modified by different methods. The experimental results showed that the catalytic performance of the catalyst was significantly improved by using the acidified and dissociated ATP. In more detail, ceria and tungsten active species were uniformly dispersed on the ATP surface. Furthermore, by various characterizations, the SCR performance, the resistance to H_2O and SO_2 properties, surface components were investigated of the CeO_2–WO_3/20%ATP-TiO_2 catalysts, of which ATP was modified by different methods. This work suggested that the catalyst prepared by using the acidified and dissociated ATP showed excellent SCR performance and tolerance to H_2O and SO_2 properties.

2 Experimental

2.1 Sample Preparation

All of the catalysts were prepared by the impregnation method. Figure 1 showed the preparation process of the catalysts. In this work, first of all, the ATP of 93% purity was dissociated and acidified. More specifically, 0.6 g dispersant sodium hexametaphosphate was dissolved in 150 mL H_2O to form a solution. Under magnetic stirring, 15 g ATP was added to the above solution and fully stirred, 1 h magnetic stirring and 30 min ultrasonic vibration were alternately carried out twice to make it fully dispersed. After 4 h of rest, the upper suspension was taken and repeated for three times. The combined suspension was centrifuged (10,000 r/min, 3 min), and the centrifugally dehydrated ATP was dried in an oven at 90 °C for 12 h, then ground and set aside. At this time, the modified ATP was denoted as dissociated ATP. Further, the 4 g dissociated ATP or 4 g ATP was dispersed in 40 g of 2 mol/L hydrochloric acid, respectively. Then stirring in a magnetic agitator for 4 h, and washed repeatedly with distilled water to the solution of pH 6, followed by centrifuging (5000 r/min-10 min), the obtained solid precipitate

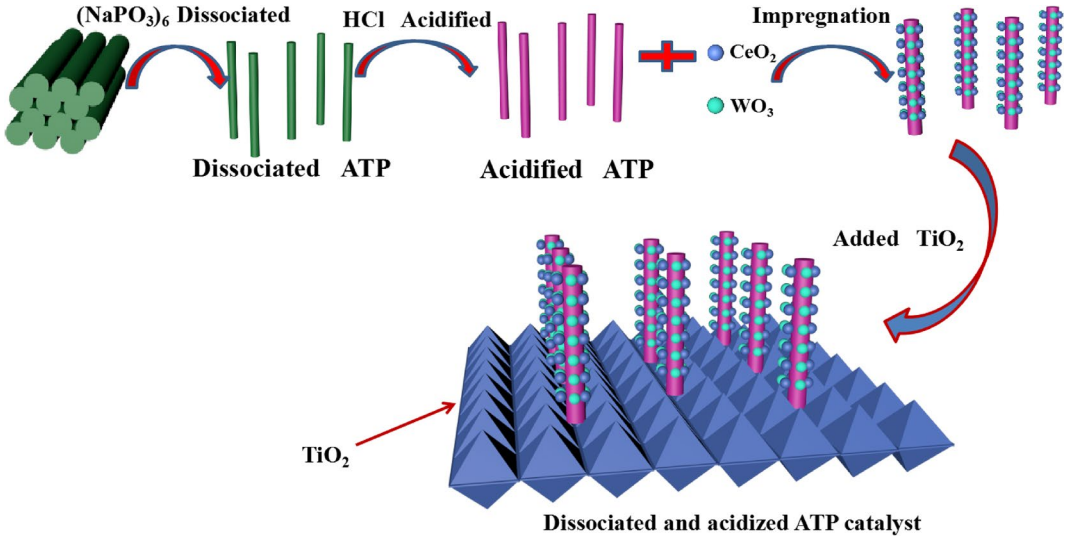

Fig. 1 Schematic diagram for the synthesis process of CAT-c

dried at 105 °C for 4 h, then ground and set aside. The modified ATP was denoted as dissociated and acidized ATP, and acidized ATP, respectively.

The CeO_2–WO_3/20%ATP-TiO_2 catalysts were prepared using different ATP by a common impregnation method. 0.505 g $Ce(NO_3)_3{\cdot}6H_2O$ and 0.106 g $(NH_4)_6H_2W_{12}O_{40}{\cdot}xH_2O$ were dissolved in 4.0 mL deionized water under magnetic stirring, and then joined 0.4 g unmodified ATP or modified in the above solution, titanium dioxide as a titanium source and then was gradually added to the above solution, Finally, stirring in a magnetic agitator for 6 h, the resulting compounds were dried in an oven at 110 °C for 12 h, calcined in 500 °C muffle furnace for 5 h with a rate of 5 °C min^{-1}. All four catalysts were CeO_2 (10 wt%)-WO_3 (5 wt%)/ATP (20 wt%)-TiO_2, the catalyst prepared by adding unmodified ATP was denoted as CAT-a. Similarly, the other catalysts prepared by adding modified ATP (dissociated ATP, dissociated and acidized ATP, and acidized ATP) were denoted as CAT-b, CAT-c and CAT-d, respectively.

2.2 Catalytic Activity Measurements

The NH_3-SCR activity measurement was tested in a fixed bed reactor, and 0.40 g catalyst (20–40 mesh) was carried out at a gas hourly space velocity (GHSV) of 30,000 h^{-1}. The reaction simulated gas were consisted of 500 ppm NO, 500 ppm NH_3, 5 vol% H_2O (when used), 100 ppm SO_2 (when used), 5 vol% O_2 and balance N_2. In addition, the total flow rate was 200 mL min^{-1}. When each reaction temperature finished, the concentration of NO_x was recorded by a KM9506 flue gas analyzer. The NO_x conversion was calculated according to the following expression:

$$\text{NO conversion} = \frac{[\text{NO}]_{\text{in}} - [\text{NO}]_{\text{out}}}{[\text{NO}]_{\text{in}}} \times 100\%$$

Where $[NO]_{in}$ represent the original NO concentration of simulated gas, while $[NO]_{out}$ represent the final NO concentration after the catalytic reaction, respectively.

3 Results and Discussion

3.1 Catalysts Characterization

The SCR activity of CAT-a, CAT-b, CAT-c, and CAT-d were shown in Fig. 2. As can be seen from Fig. 2, in the

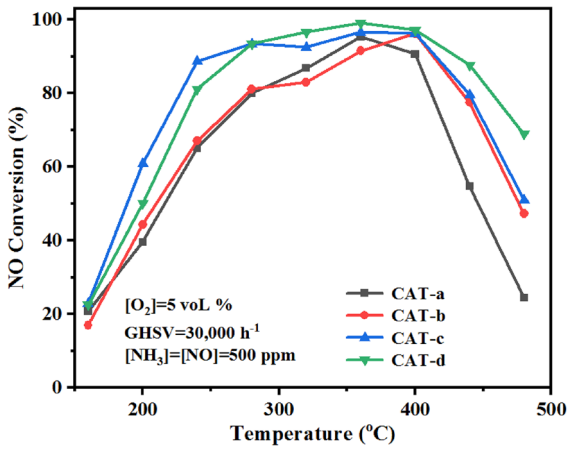

Fig. 2 NO_x conversion of the catalysts during 160–480 °C. Reaction conditions: [NO] = [NH_3] = 500 ppm, [O_2] = 5 vol%, balance N_2 and GHSV = 30,000 h^{-1}

temperature range of 160–280 °C, the treated ATP catalysts had better catalytic activity than the CAT-a. Furthermore, the CAT-c exhibited the best catalytic performance at 160–280 °C. In more detail, the NO_x conversion of the CAT-c could reach to 88.7% at 240 °C, and the maximum NO_x conversion was 96.6% at 360 °C. Besides, the CAT-a had significantly decreased at 400–480 °C. However, the NO_x conversion of the CAT-c still could maintain above 79% at 440 °C. Therefore, the CAT-c showed the best catalytic performance at medium and low temperatures.

3.2 H_2O and SO_2 Resistant Properties

When H_2O and SO_2 existed in the flue gas, the low-temperature SCR reaction would be affected to a certain extent. Therefore, it was necessary to study the influence of H_2O and SO_2 on catalysts SCR performance. Figure 3a showed the results of H_2O resistance of CAT-b and CAT-c. For CAT-b and CAT-c, within 0.5 h before the water was not pumped, the NO_x conversion of the two catalysts remained stable. After 1 h, when the H_2O was pumped, the NO_x conversion of the CAT-c slightly increased. However, the NO_x conversion of the CAT-b significantly decreased from 84.5 to 78.3%. Within the next 7 h, the NO_x conversion of the CAT-c could be maintained above 90%, while the NO_x conversion of the CAT-b declined to below 80%. When the H_2O was turned off, the SCR performance of the CAT-c was basically stable, and the catalytic activity of the CAT-b had gradually risen. On the whole, after entering the water, the catalytic activity of the CAT-c was better than the CAT-b. Therefore, the CAT-c had excellent H_2O resistance performance.

Besides, the results of SO_2 resistance of CAT-b and CAT-c were shown in Fig. 3b. For the CAT-c, in the 1 h, when SO_2 was pumped, the NO_x conversion decreased from 92.5 to 84.9%. Although the NO_x conversion of the CAT-c was a little decreased. Then, in the next 7 h, the NO_x conversion could be stabilized above 80%. This may be because after the ATP was dissociated and acidified, the dispersion and specific surface area of the rod crystals were improved, and more surface active groups were released. While

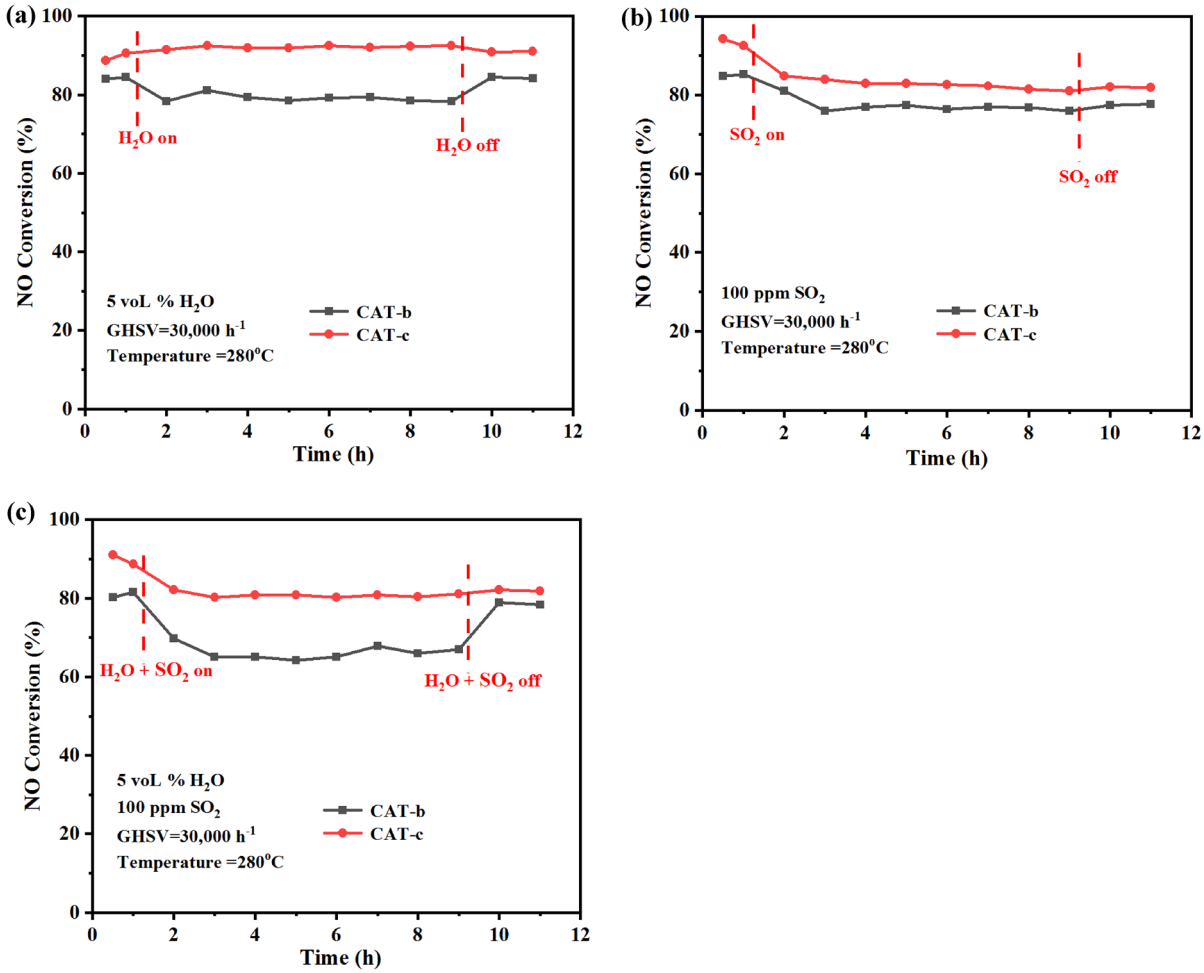

Fig. 3 H_2O tolerance test (**a**), SO_2 tolerance test (**b**), H_2O and SO_2 tolerance test (**c**) of the two catalysts at 280 °C, 5% O_2, GHSV = 30,000 h^{-1}

acidizing treatment can remove impurities in ATP channels and dredge the channels, and H^+ can replace the Mg^{2+}, Al^{3+} and other metal ions contained in ATP, which improved the cation exchange ability of ATP. Therefore, these effects were helpful to improve the adsorption performance of ATP, and the SO_2 resistance of CAT-c was further improved. Besides, when SO_2 was stopped, the catalytic performance of the catalyst had been slightly improved. However, for the CAT-b, in the 2 h, when SO_2 was pumped, the NO_x conversion had a marked decline, and from 85.3% declined to 76.0%. In the following 6 h, the NO_x conversion only kept at about 77%. When SO_2 was stopped, the catalytic activity of the CAT-b had a faint enhancement. In a word, after adding the SO_2, the CAT-c showed more excellent SO_2 resistance performance.

Furthermore, in the presence of both H_2O and SO_2, the catalytic performance of two catalysts was shown in Fig. 3c. For the CAT-c, in the 1 h, when H_2O and SO_2 were both turned on, the NO_x conversion decreased from 88.7 to 82.1%. Then, in the next 7 h, the NO_x conversion could be stabilized above 80%. Besides, when H_2O and SO_2 were both stopped, the NO_x conversion had gradually recovered to around 82%. However, for the CAT-b, in the 2 h, when H_2O and SO_2 were both pumped, the NO_x conversion had a significant decline, and from 81.5% declined to 65.1%. In the following 6 h, the NO_x conversion only kept at about 65%. When H_2O and SO_2 were both turned off, the NO_x conversion of the CAT-b could only be restored to about 80%. Therefore, it could be concluded that the CAT-c had satisfactory H_2O and SO_2 resistance performance.

3.3 Structure of the Catalyst

Figure 4 showed the XRD results of the four catalysts, and it was obvious that the four catalysts had similar diffraction peaks. In more detail, four catalysts showed nine distinct peaks at 25.25, 37.78, 48.03, 53.89, 55.06, 62.65, 68.89, 70.30 and 75.12°, corresponding to the (101), (004), (200), (105), (211), (204), (116), (220) and (215) lattice planes of anatase TiO_2 (PDF#75-1537). Moreover, four catalysts also showed two peaks at 28.53 and 33.06°, which indexed to the (111) and (200) crystal planes of cubic CeO_2 (PDF#81-0792). However, none of the four catalysts showed the diffraction peak of the WO_x phase, indicating that tungsten oxides were highly dispersed on the surfaces of the four catalysts.

Figure 5 showed the SEM images of CAT-a and CAT-c. In more detail, some particles can be seen in the CAT-a SEM images (Fig. 5a). These particles may be some calcium salt impurities, and the content of CaO was 0.195% (Table S1). Which also showed that CAT-a was symbiotic with calcium salt. Meanwhile, the CAT-a rod crystals were gathered together (Fig. 5b).

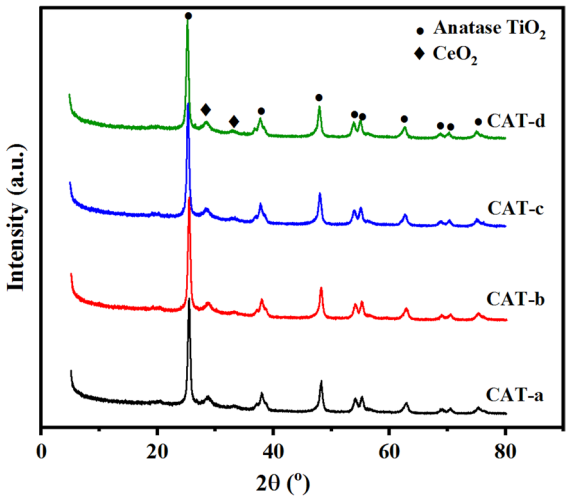

Fig. 4 XRD spectroscopy of the four catalysts

For CAT-c, some particles were significantly decreased (Fig. 5c). This may be because HCl had removed some calcium salt impurities from the attapulgite. At this time, the content of CaO was 0% (Table S1). Besides, the attapulgite was needle-like and fibrous of CAT-c, and the rod crystals were dispersed (Fig. 5d), which may be due to the action of $(NaPO_3)_6$, the rod crystals were dissociated, and forming dispersed fibers.

Figure 6 showed the TEM results of CAT-a and CAT-c. The lattice fringes with a different lattice spacing of the CAT-a could be clearly seen in Fig. 6a. Typically, the d = 0.35 nm value of lattice fringes could be attributed to the (101) plane of anatase TiO_2 (PDF#21-1272). Meanwhile, the lattice fringes of d = 0.31 nm corresponding to the CeO_2 (111) plane (PDF#34-0394). The dispersion of active species of CAT-a was exhibited in Fig. 6b. For comparison, Fig. 6c showed the active cerium species of CAT-c was uniformly dispersed on the surface of ATP, and the lattice fringes of d = 0.27 nm corresponding to the CeO_2 (200) plane, which showed that the CeO_2 lattice spacing of CAT-c slightly decrease. Besides, the dispersion of active species and the clear diffraction ring were exhibited in Fig. 6d, which also showed that the active species were well dispersed on the surface of the CAT-c. To further prove, Fig. 6e–l showed the Ce, W, Ti, O, Si, Mg, and Al elements EDS mapping results of CAT-c. It was clearly seen that a small number of active species cerium and tungsten were uniformly dispersed on the ATP surface, and the rest were dispersed in the channel of TiO_2. In a word, the good dispersion and excellent structure of catalysts played an important role in SCR reaction. Therefore, the CAT-c showed excellent catalytic performance.

The Fig. 7a showed the N_2 adsorption–desorption curves of the four catalysts. According to IUPAC classification, the four catalysts curves were belonged to type IV with H2

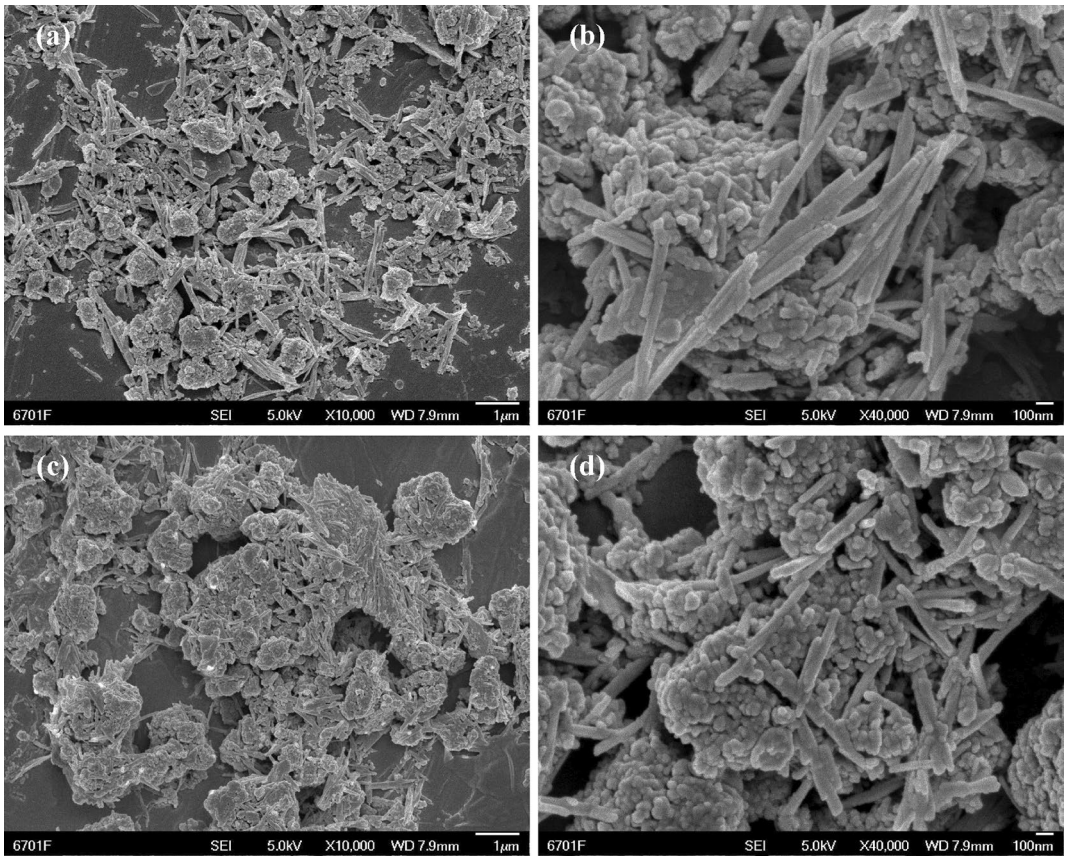

Fig. 5 SEM micrographs of the CAT-a (**a**, **b**), CAT-c (**c**, **d**)

hysteresis loop, indicating that the four catalysts had typical mesoporous structure. Due to the existence of a mesoporous structure, the pore volumes and average pore diameter of the four catalysts were further analyzed. As shown in Table 1, the pore volumes of CAT-a, CAT-b, CAT-c and CAT-d were 0.32 $cm^3\ g^{-1}$, 0.32 $cm^3\ g^{-1}$, 0.33 $cm^3\ g^{-1}$, and 0.32 $cm^3\ g^{-1}$, respectively. Moreover, the average pore diameter of CAT-a, CAT-b, CAT-c and CAT-d were 13.33 nm, 13.19 nm, 13.64 nm, and 13.16 nm, respectively. For CAT-b and CAT-d, the average pore diameter were all slightly decreased. However, the average pore diameter of CAT-c increased significantly. This may be because of the effect of $(NaPO_3)_6$ on attapulgite, the fiber bundles were dissociated. And attapulgite in the process of acid acidification, some calcium salt or impurities were removed from attapulgite channels. It was obvious that the 0.195% of calcium salt was removed (Table S1). Therefore, the average pore diameter of CAT-c had an obvious increase.

Furthermore, the pore size distribution curves of CAT-a, CAT-b, CAT-c and CAT-d were shown in Fig. 7b. Obviously, the pore size distribution of the four catalysts was concentrated at 2–50 nm. The results showed that the four catalysts had a mesoporous structure. In short, the large average pore diameter and typical mesoporous structure of the CAT-c played a crucial role in SCR performance.

3.4 Catalysts Reducibility

The H_2-TPR profiles of CAT-a, CAT-b, CAT-c and CAT-d were shown in Fig. 8. For the six catalysts, the onset temperature of H_2 consumption was 300 °C, and none of them show the peaks of TiO_2 and WO_3. Moreover, the CeO_2 reduction peaks of the four catalysts appeared at 594 °C, 576 °C, 588 °C, and 579 °C, respectively. This could be attributed to the reduction of surface Ce^{4+} to Ce^{3+} [33–35]. Meanwhile, they all had other CeO_2 peaks at 682 °C, which could be accounted for the reduction of bulk CeO_2 [34]. Compared with the CAT-a, the first reduction peak of treated ATP catalysts moved to a lower temperature range. In more detail, the first reduction peak of the CAT-c slightly shifted to a lower temperature. It may be because ATP was dissociated by using $(NaPO_3)_6$ and acidified by using HCl, the interaction between cerium oxide species and TiO_2 was strengthened. Therefore, the reduction ability of the CAT-c was promoted. It is well known that the reduction performance of the catalysts was directly affected by the peak positions [24]. The

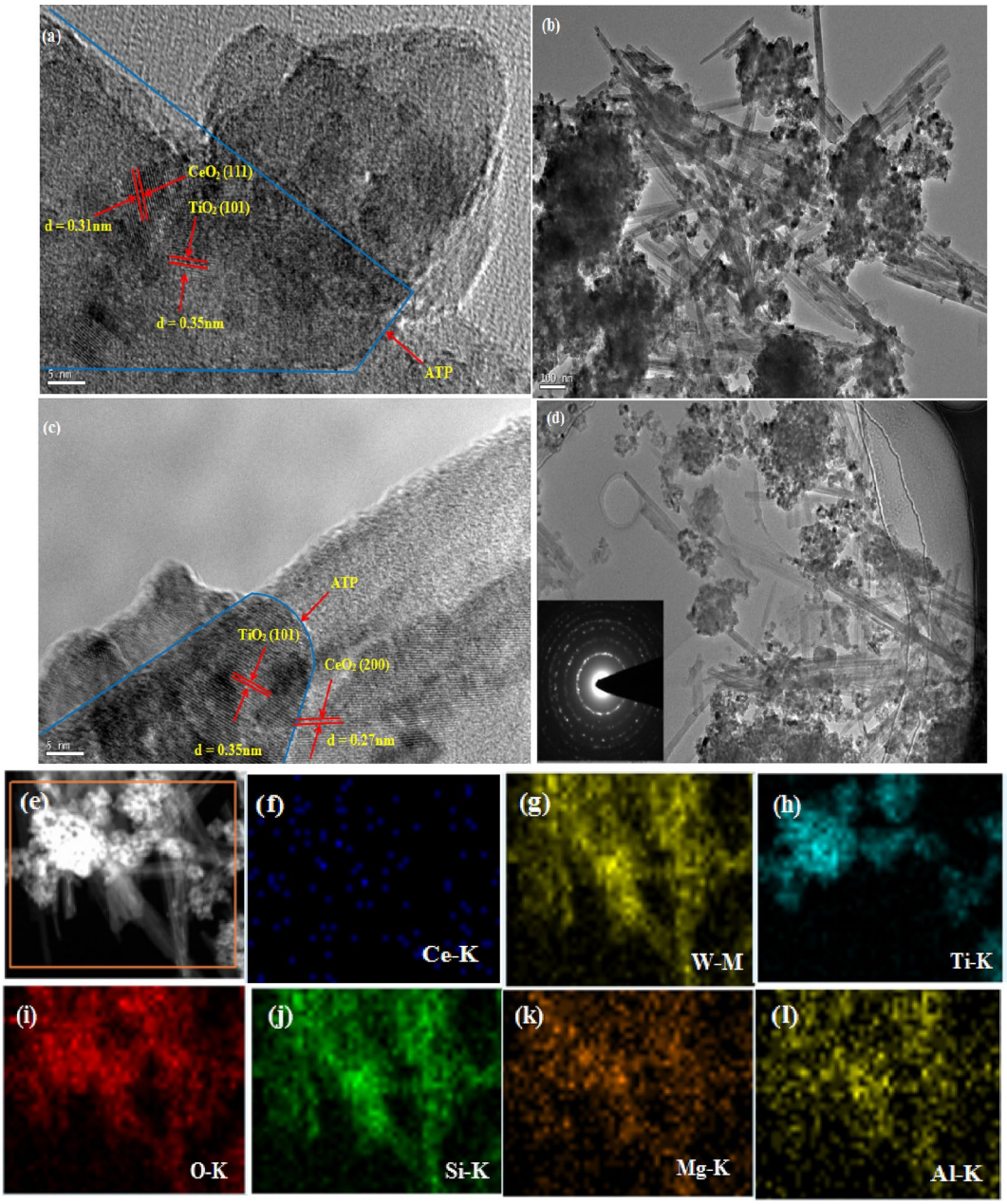

Fig. 6 HRTEM and TEM images: **a**, **b** CAT-a; **c**, **d** CAT-c; EDS mapping of the CAT-c (**e**–**l**)

lower reduction temperature of the CAT-c was consistent with higher SCR catalytic activity, which played a crucial role in CAT-c SCR reaction.

To further study the chemical states of surface elements, XPS spectra were investigated for the CAT-a, CAT-c and CAT-c after H_2O and SO_2 test. The surface element concentrations of the three catalysts were listed in Table 2. It can be seen that the CAT-c (1.62%) had a lower Ce concentration than the CAT-a (1.66%). It showed that after $(NaPO_3)_6$ dissociation and HCl acidification of ATP, the adsorption capacity of the prepared CAT-c may be enhanced. Therefore, the CAT-c can adsorb more active species cerium into the ATP channel. As a result, the CAT-c showed a lower Ce concentration.

The Ce 3d XPS results of the CAT-a and the CAT-c were shown in Fig. 9a. In more detail, the Ce 3d consisted of eight peaks, which were v (882.4 eV), v′ (885.9 eV), v″ (889.8 eV), v‴ (898.7 eV), u (901.3 eV), u′ (904.5 eV), u″ (907.8 eV) and u‴ (917.1 eV) [36, 37], respectively. Meanwhile, the peaks of v′ and u′ could represent the $3d^{10}4f^1$ initial electronic state, which was assigned to Ce^{3+} species. And the other peaks could express the $3d^{10}4f^0$ state, which

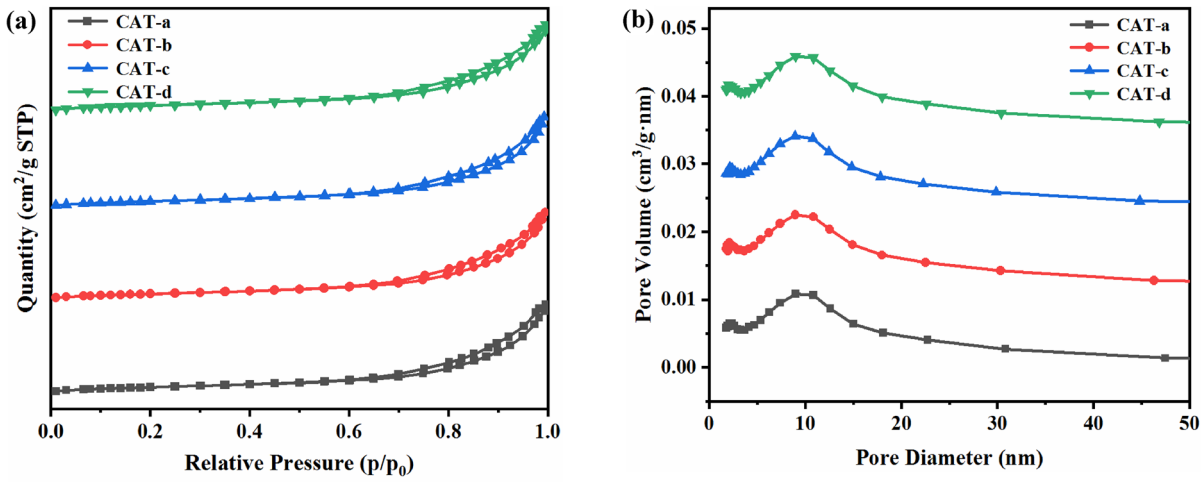

Fig. 7 N_2 adsorption–desorption isotherms of the four catalysts (**a**); Pore size distribution of the four catalysts (**b**)

Table 1 Surface area, pore characteristics of the four catalysts

Catalyst	S_{BET}(m^2 g^{-1})	Pore volume(cm^3 g^{-1})	Average pore diameter(nm)
CAT-a	84.09	0.32	13.33
CAT-b	83.57	0.32	13.19
CAT-c	86.33	0.33	13.64
CAT-d	86.52	0.32	13.16

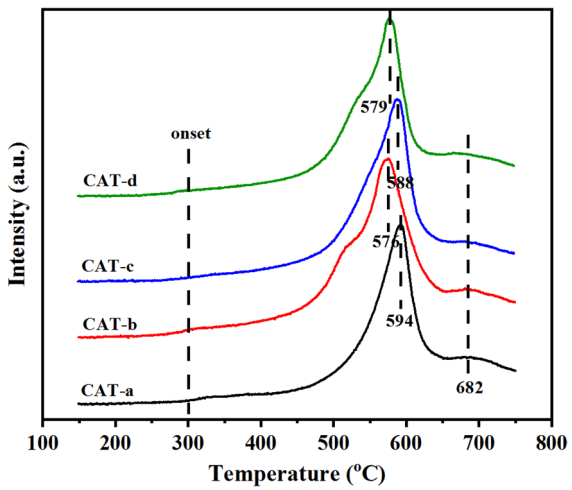

Fig. 8 H_2-TPR profiles of different the catalysts

was attributed to Ce^{4+} species [38]. Table 2 calculated the $Ce^{3+}/(Ce^{3+} + Ce^{4+})$ atomic ratio results of the three catalysts. For the CAT-a and the CAT-c, the $Ce^{3+}/(Ce^{3+} + Ce^{4+})$ atomic ratio was 35.82% and 30.93%, respectively. Compared with the CAT-a, the peak positions of the CAT-c shifted to the higher binding energy. The change may be assigned to the strong interaction between CeO_2 and the dissociated and acidized ATP, it was consistent with the above adsorption explanation.

Fig. S1(a) showed the Ce 3d XPS results of the CAT-c and the CAT-c after H_2O and SO_2 test. According to the Table 2, the CAT-c (30.93%) had a higher Ce^{3+} ratio than the CAT-c after H_2O and SO_2 test (29.86%). This showed that the conversion between Ce^{4+} and Ce^{3+} was more frequent within the CAT-c. Besides, the higher Ce^{3+} ratio was more beneficial to the fluidity of chemisorption oxygen [39]. Therefore, the CAT-c had a better fluidity of chemisorption oxygen.

The O 1s XPS results of two catalysts were shown in Fig. 9b. For the O 1s, it was divided into two peaks. The binding energy peaks from 529.44 to 530.90 eV were attributed to lattice oxygen O_β, and the binding energy peaks from 531.00 to 532.50 eV were assigned to chemical adsorbed oxygen O_α [40]. The Table 2 showed the $O_\alpha/(O_\alpha + O_\beta)$ atomic ratio results of the three catalysts. In more detail, the $O_\beta/(O_\alpha + O_\beta)$ atomic ratio (39.93%) of the CAT-c was slightly higher than the CAT-a (35.53%). This

Table 2 XPS results of the three catalysts for surface atomic concentration (%)

Sample	Ce	W	Ti	O	Si	Mg	Al	S	N	$O_\alpha/(O_\alpha+O_\beta)$	$Ce^{3+}/(Ce^{3+}+Ce^{4})$
CAT-a	1.66	1.76	9.61	59.73	16.35	4.23	6.66	–	–	64.47	35.82
CAT-c	1.62	1.79	10.21	60.21	16.38	2.34	7.45	–	–	60.07	30.93
CAT-c after H_2O and SO_2 test	1.27	1.74	10.11	57.95	15.83	1.85	7.38	1.93	1.94	59.23	29.86

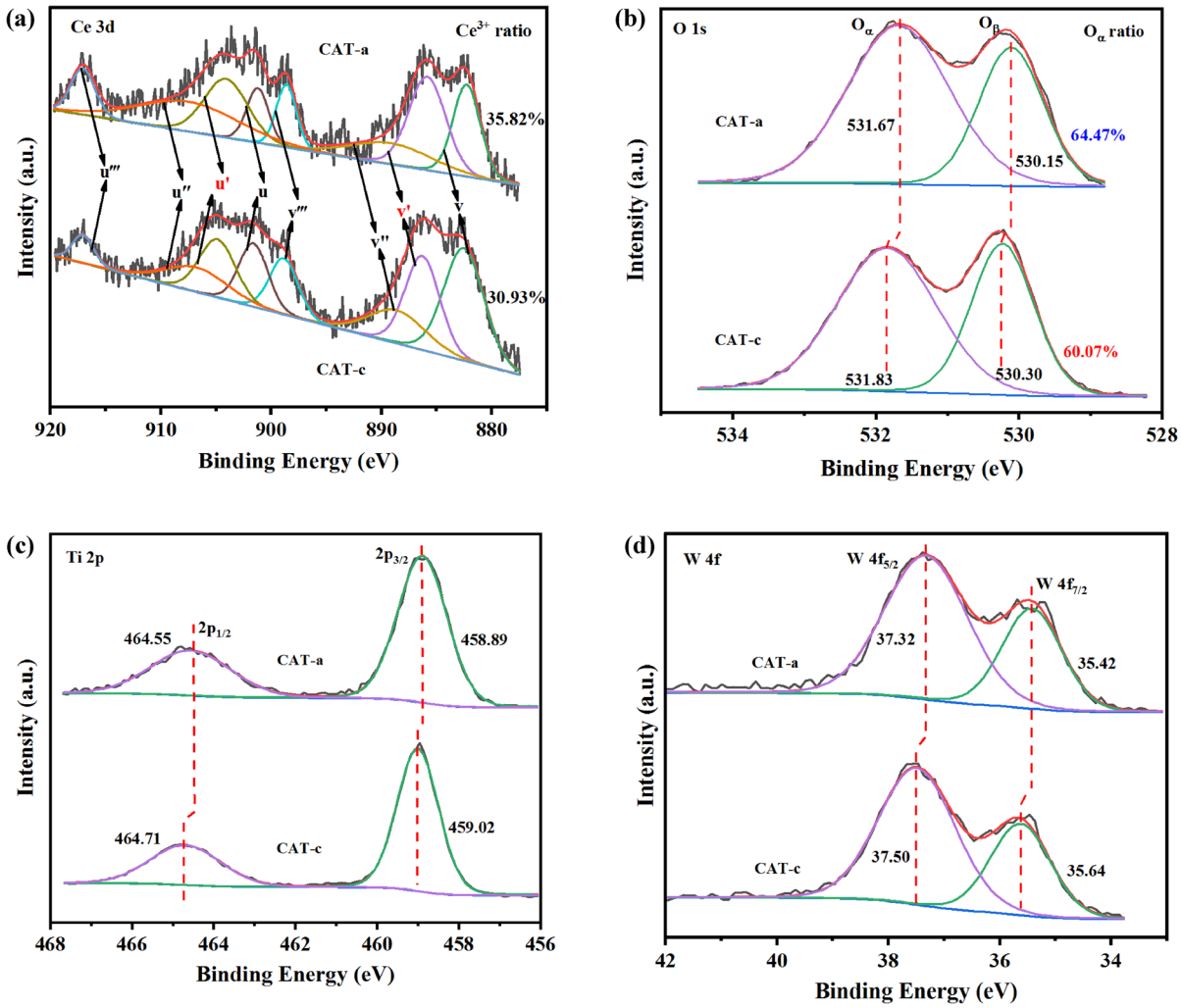

Fig. 9 XPS results about Ce 3d (**a**), O 1s (**b**), Ti 2p (**c**) and W 4f (**d**) of CAT-a, and CAT-c

showed that there were more low-coordination atoms on the TiO_2 (001) facets in the CAT-c [41]. Therefore, the catalytic activity of the CAT-c was improved. For the CAT-a and the CAT-c, the $O_\alpha/(O_\alpha+O_\beta)$ atomic ratio was 64.47% and 60.07%, respectively. It is well known that chemisorption of oxygen plays a crucial role in SCR [36]. However, the CAT-c had better catalytic activity, the increase of chemical adsorbed oxygen did not increase the CAT-a SCR activity. This may be because the CAT-a contained more calcium salt impurities (Table S1).

Compared the CAT-c with the CAT-c after H_2O and SO_2 test (Fig. S1(b)), the $O_\alpha/(O_\alpha+O_\beta)$ atomic ratio of the two catalysts was 60.07% and 59.23%, respectively. When the H_2O and SO_2 were pumped, the O_α atomic ratio of the CAT-c after H_2O and SO_2 test was reduced. Therefore, in the process of water and sulfur resistance, the catalytic activity of the CAT-c after H_2O and SO_2 test was decreased.

Figure 9c showed the Ti 2p XPS results of two catalysts. In more detail, the binding energies of Ti $2p_{3/2}$ (458.53 eV) and Ti $2p_{1/2}$ (464.24 eV) were assigned to the peaks of Ti^{4+} ions [42]. Comparison of Ti 2p results between the CAT-a and the CAT-c, the bands of the CAT-c Ti 2p moved towards higher binding energy. This also indicated that the CAT-c had stronger titanium species interaction than that of the CAT-a.

The Ti 2p XPS results of the CAT-c and the CAT-c after H_2O and SO_2 test were shown in Fig. S1(c). Compared to the two catalysts, the Ti 2p electron bands of the CAT-c after H_2O and SO_2 test shifted to the higher binding energy. This may be because of the effect of H_2O and SO_2.

Figure 9d exhibited the W 4f XPS results of two catalysts. The W 4f consisted of two peaks. The peak of binding energy at 35.60 eV was attributed to W $4f_{7/2}$, and the peak of binding energy at 37.40 eV was assigned to W $4f_{5/2}$ [43]. For the CAT-a and the CAT-c, according to calculating,

the surface atomic ratio of W $4f_{7/2}$/(W $4f_{5/2}$ + W $4f_{7/2}$) was 33.39% and 34.46%, respectively. This also showed that with the increase of the W $4f_{7/2}$/(W $4f_{5/2}$ + W $4f_{7/2}$) atomic ratio, the catalytic activity of the CAT-c also increased. The results showed that tungsten species had strong interaction with attapulgite and titanium dioxide carriers, so the catalytic activity of the CAT-c was greatly improved. For the CAT-c and the CAT-c after H_2O and SO_2 test, the W 4f XPS results were shown in Fig. S1(d). The atomic ratio of W $4f_{7/2}$/(W $4f_{5/2}$ + W $4f_{7/2}$) was 34.46% and 34.24%, respectively. Combined with the catalytic activity results of the two catalysts, and the catalytic activity of the CAT-c after H_2O and SO_2 test was decreased. This may be because the interaction between tungsten species, attapulgite and titanium dioxide carriers was weakened in the process of water and sulfur resistance. Therefore, the W $4f_{7/2}$ ratio may be related to the catalytic activity of the catalysts.

The Si, Mg and Al elements XPS results of two catalysts were shown in Fig. S1(e–g). For the CAT-c after H_2O and SO_2 test, the Si, Mg and Al elements peak positions moved towards the lower binding energy. ATP is made of a variety of components, such as Si, Mg and Al species. Due to the addition of H_2O and SO_2, the interaction between the active species and the ATP carrier was further weakened. Therefore, the binding energy peaks moved to the lower binding energy direction.

3.5 FTIR Spectroscopy

In addition, to further study the surface functional groups of the catalysts. Figure 10 exhibited the FTIR results of four catalysts. For the four catalysts, they all had the same characteristic peaks at 1029 cm^{-1} and 1632 cm^{-1}, which could correspond to the stretching vibration of Si–O bond in ATP and the nitrate species, respectively [44]. However, for the CAT-a, the peak at 2360 cm^{-1} might be assigned to the adsorbed CO_2 stretching vibration [45]. Besides, for the CAT-a and CAT-c, the peak positions appeared at 3410 cm^{-1}, which could ascribe to the stretching vibration of absorbed water [46]. Finally, for the CAT-b and CAT-d, the bands at 3421 cm^{-1}, which were interpreted as the stretching vibration of –OH bond [47].

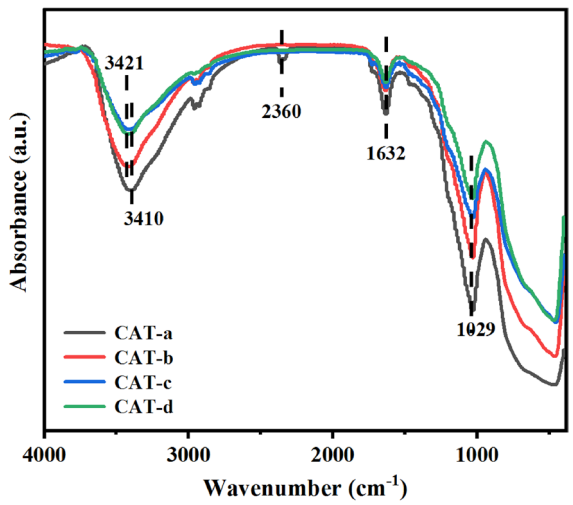

Fig. 10 The FTIR spectra results of the four catalysts

4 Conclusions

In this paper, a series of CeO_2–WO_3/20%ATP-TiO_2 catalysts were synthesized, of which ATP was modified by different methods. Notably, the acidified and dissociated ATP can enhance the absorption performance of active components and strengthen the interaction between CeO_2, WO_3 and TiO_2. Therefore, the CAT-c prepared exhibited satisfactory performance for selective catalytic reduction (SCR) NO_x with NH_3 and better adsorption performance. And the CAT-c also showed strong tolerance to H_2O and SO_2. In a word, the high dispersion of active species, the SCR performance of the catalyst was significantly improved by using the acidified and dissociated ATP. Therefore, the CAT-c will have a broad application prospect in the preparation of other metal oxide catalysts and even in other catalytic fields.

Supplementary Information The online version contains supplementary material available at https://doi.org/10.1007/s10563-021-09330-y.

Acknowledgements This work was supported by the National Natural Science Foundation of China (51808529), the Major Project of Inner Mongolia Science and Technology (2019ZD018), the Foundation of Key Laboratory of Clay Mineral Applied Research of Gansu Province, Lanzhou Institute of Chemical Physics, Chinese Academy of Sciences (CMAR-2019-3), the Science and Technology Program of Chengguan district, lanzhou city (2019JSCX0042), and the DNL Cooperation Fund, CAS (DNL201906).

References

1. Meng D, Zhan W, Guo Y, Guo Y, Wang L, Lu G (2015) ACS Catal 5:5973–5983
2. Zhang D, Zhang L, Shi L, Fang C, Li H, Gao R, Huang L, Zhang J (2013) Nanoscale 5:1127–1136
3. Yang Q, Wang Y, Zhao C, Liu Z, Gustafson WI Jr, Shao M (2011) Environ Sci Technol 45:6404–6410
4. Liu J, Li X, Zhao Q, Hao C, Wang S, Tade M (2014) ACS Catal 4:2426–2436
5. Li X, Li J, Peng Y, Li X, Li K, Hao J (2016) J Phys Chem C 120:18005–18014
6. Li X, Li J, Peng Y, Zhang T, Liu S, Hao J (2015) Catal Sci Technol 5:4556–4564
7. Huang X, Zhang G, Lu G, Tang Z (2018) Catal Surv Asia 22:1–19
8. Shan W, Geng Y, Chen X, Huang N, Liu F, Yang S (2016) Catal Sci Technol 6:1195–1200
9. Chen L, Weng D, Si Z, Wu X (2012) Prog Nat Sci 22:265–272

10. Zhang G, Han W, Zhao H, Zong L, Tang Z (2018) Appl Catal B 226:117–126
11. Ding S, Liu F, Shi X, He H (2016) Appl Catal B 180:766–774
12. Wang X, Li X, Zhao Q, Sun W, Tade M, Liu S (2016) Chem Eng J 288:216–222
13. Jiang Y, Bao C, Liu Q, Liang G, Lu M, Ma S (2018) Catal Commun 103:96–100
14. Huang X, Zhang H, He M (2017) Gene 637:1–8
15. Shan W, Liu F, Yu Y, He H (2014) Chin J Catal 35:1251–1259
16. Qi G, Yang R, Chang R (2004) Appl Catal B 51:93–106
17. Shen B, Ma H, He C, Zhang X (2014) Fuel Process Technol 119:121–129
18. Shan W, Liu F, He H, Shi X, Zhang C (2012) Appl Catal B 100:115–116
19. Jiang Y, Xing Z, Wang X, Huang S, Wang X, Liu Q (2015) Fuel 151:124–151
20. Gao X, Jiang Y, Fu Y, Zhong Y, Luo Z, Cen K (2010) Catal Commun 11:465–469
21. Xu W, He H, Yu Y (2009) J Phys Chem C 113:4426–4432
22. Huang H, Shan W, Yang S, Zhang J (2014) Catal Sci Technol 4:3611–3614
23. Zhu L, Zhong Z, Yang H, Wang C (2017) Environ Technol 38:1285–1294
24. Zhou X, Huang X, Xie A, Luo S, Yao C, Li X, Zuo S (2017) Chem Eng J 326:1074–1085
25. Lu Y, Dong W, Wang W, Wang Q, Hui A, Wang A (2019) Appl Clay Sci 167:50–59
26. Li X, Yin Y, Yao C, Zuo S, Lu X, Luo S, Ni C (2016) Particuology 26:66–72
27. Xie A, Zhou X, Huang X, Ji L, Zhou W, Luo S, Yao C (2017) J Ind Eng Chem 49:230–241
28. Wang F, Wang W, Zhu Y, Wang A (2017) J Rare Earth 35:697–708
29. Huang X, Xie A, Wu J, Xu L, Luo S, Xia J, Yao C, Li X (2018) J Mater Res 33:3559–3569
30. Xie W, Zhang G, Mu B, Tang Z, Zhang J (2020) Appl Clay Sci 192:1–10
31. Xie A, Tao Y, Jin X, Gu P, Huang X, Zhou X, Luo S, Yao C, Li X (2019) New J Chem 43:2490–2500
32. Chen C, Cao Y, Liu S, Chen J, Jia W (2019) Appl Surf Sci 480:537–547
33. Zong L, Zhang J, Lu G, Tang Z (2018) Catal Surv Asia 22:105–117
34. Peng Y, Li J, Chen L, Chen J, Han J, Zhang H, Han W (2012) Environ Sci Technol 46:2864–2869
35. Djerad S, Tifouti L, Crocoll M, Weisweiler W (2004) J Mol Catal A 208:257–265
36. Zhang G, Han W, Dong F, Zong L, Lu G, Tang Z (2016) Rsc Adv 6:76556–76567
37. Zong L, Zhang G, Zhao J, Dong F, Zhang J, Tang Z (2018) Chem Eng J 343:500–511
38. Li X, Si Y, Ji L, Gong P (2017) Ecol Model 360:70–79
39. Huang X, Zhang G, Dong F, Tang Z (2019) J Ind Eng Chem 69:66–76
40. Dupin JC, Gonbeau D, Vinatier P, Levasseur A (2000) Phys Chem Chem Phys 2:1319–1324
41. Shi Q, Li Y, Zhou Y, Miao S, Ta N, Zhan E, Liu J, Shen W (2015) J Mater Chem A 3:14409–14415
42. Du X, Gao X, Fu Y, Gao F, Luo Z, Cen K (2012) J Colloid Interface Sci 368:406–412
43. Camposeco R, Castillo S, Mugica V, Mejia-Centeno I, Marin J (2014) Chem Eng J 242:313–320
44. Zhang Z, Wang W, Wang A (2015) J Environ Sci China 33:106–115
45. Chen L, Li R, Li Z, Yuan F, Niu X, Zhu Y (2017) Catal Sci Technol 7:3243–3257
46. Chen Z, Peng Y, Chen J (2020) Environ Sci Technol 54:14465–14473
47. Mamede AS, Payen E, Grange P, Poncelet G, Ion A, Alifanti M, Parvulescu VI (2004) J Catal 223:1–12